MMW Signal Gain in DML-Based Microwave Photonic Links Under Large Signal Regime

M. Botella-Campos, J. Mora, and B. Ortega, *Senior Member, IEEE*

***Abstract*—This article presents a theoretical and experimental analysis of the millimeter wave (mmW) signal gain observed in photonically generated signals by using carrier suppressed (CS) external modulation in a centralized network architecture while the data is transmitted over a directly modulated laser (DML) operating under different signal regimes. Measurements of the frequency response under small and large signal regimes are presented for the sake of comparison. Moreover, the mmW signal gain has been measured for different standard single mode fiber (SSMF) lengths in order to identify the conditions and impact of large signal regime operation. The results are also validated by the experimental transmission of a 25 MHz QPSK signal transmitted over 40 GHz since the error-vector-magnitude (EVM) is measured for different input electrical power values as well as several received optical power (RoP) levels. Moreover, the spurious-free dynamic range (SFDR) ratio is measured to compare the third-order intermodulation distortion (IMD3) between small and large signal regime. The quantitative results demonstrate that proper system conditions allow the exploitation of the mmW signal gain towards the future deployment of high energy efficient networks.**

***Index Terms*—Intermodulation, microwave photonics, millimeter wave, optical access networks, radio access networks.**

I. Introduction

THE continuous growth of total mobile traffic at an estimated annual rate of 55% in 2020–2030 leads to 543 EB per month in 2025 and 4394 EB in 2030. The main drivers for this increase are the device proliferation, i.e., 29.3 billion networked devices by 2023 [1], the extensive usage of high-resolution video-on-demand services, the increase of machine–to-machine (M2M) applications and the higher demand of mobile cloud services [2].

Such explosive traffic growth requires the adoption of several strategies including the increase of spectrum availability and energy efficiency, the network densification with smaller cells and higher volume of traffic offloading towards local area networks (LAN). Therefore, millimeter wave (mmW) technology, already introduced by the fifth generation (5G) new radio (NR), is still essential in sixth generation (6G) networks due to the huge bandwidth, as well as new air interface and the deployment of open-radio access networks (O-RAN) as a new architecture to build a virtualized resource efficient, cost effective, software-driven, centralized, slicing-aware, open source, more flexible and dynamic radio network than previous generations of mobile networks [3].

Analog-radio-over-fiber (A-RoF) solutions provide seamlessly transport of mmW signals to keep transparency to wireless users. Thus, cost-efficient, low latency and large bandwidth links can be deployed in future O-RAN where the availability and costs of the optical infrastructure become critical, especially due to small-cell environment [4]. The centralized network architecture hosts the baseband units (BBUs) at the central office (CO) where medium access control (MAC) layer functions, digital-to-analog and analog-to-digital conversion (DAC/ADC), radio frequency (RF) frontends and baseband processing are performed. Therefore, broad coverage is provided due to the large number of remote radio heads (RRH) connected to a centralized BBU pool with a span fiber link while only opto-electronic conversion and electronic amplification is held at the simplified RRHs [5].

In the literature, a large number of microwave photonics based approaches has been proposed for low phase noise and frequency tunable signal generation by using electronic components with reduced bandwidth [6], [7]. As one of the most attractive options, optical frequency multiplication by using an external Mach-Zehnder modulator (MZM) biased at carrier suppression (CS) point offers easy implementation, high quality, flexible and efficient mmW signal generation [8], [9] over data directly modulated laser (DML)-based links.

Previous work on theoretical and experimental CS-MZM remote approach, i.e., located at the CO, under small signal regime demonstrated a significant gain in the photonically generated mmW band which can be exploited for future deployment of energy-efficient networks [10]. More concretely, 15 dB gain was demonstrated due to the combined effect of 25 km fiber dispersion and the DML chirp in the 40 GHz-band frequency response with the subsequent improvement in data transmission performance, and oppositely to the system baseband behavior.

However, the impact of harmonic and intermodulation distortion in remotely generated mmW signal limits the overall system performance [11] and linearization techniques might be considered for reducing DML induced HD and IMD [12]. Indeed, the system response will be significantly different under

Manuscript received 31 December 2022; revised 5 April 2023; accepted 5 May 2023. Date of publication 18 May 2023; date of current version 19 September 2023. This work was supported in part by MCIN/AEI/ 10.13039/501100011033 and ERDF A way of making Europe under Grant PID2021-126514OB-I00 OPTIMISE, and in part by Generalitat Valenciana through Project PROMETEO 2021/015. *(Corresponding author: M. Botella-Campos.)*

This work did not involve human subjects or animals in its research.

The authors are with the Instituto de Telecomunicaciones y Aplicaciones Multimedia, ITEAM, Universitat Politècnica de València, 46022 Valencia, Spain (e-mail: marbocam@teleco.upv.es; jmalmer@iteam.upv.es; bortega@dcom.upv.es).

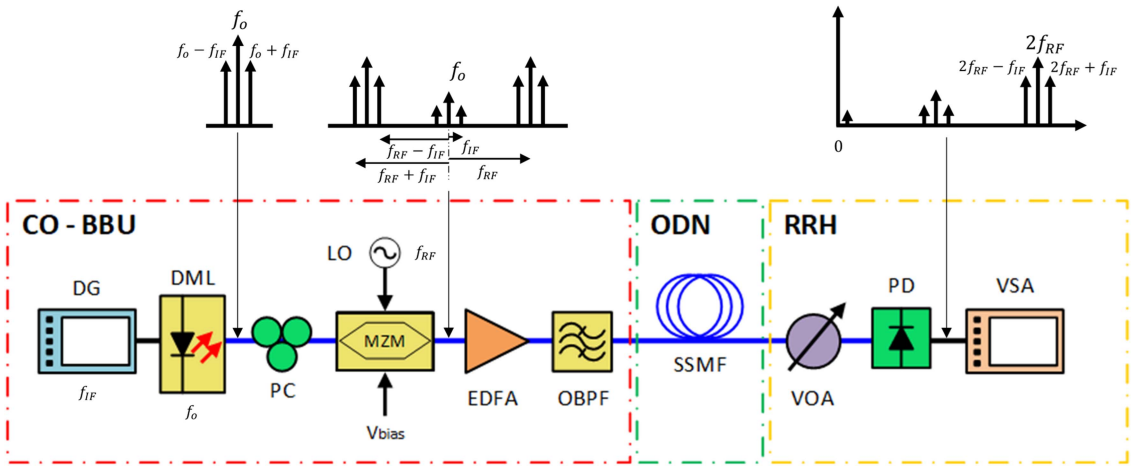

Fig. 1. Experimental setup for DML signal transmission over CS-MZM based mmW generated signal. CO-BBU: Baseband unit at the central office, DG: Digital generator, DML: Directly modulated laser, PC: Polarization controller, LO: Local oscillator, MZM: Mach-Zehnder modulator, EDFA: Erbium doped amplifier, OBPF: Optical band pass filter, ODN: Optical distribution network, SSMF: Standard single mode fiber, RRH: Remote radio head, VOA: Variable optical attenuator, PD: Photodetector, VSA: Vectorial signal analyzer.

large signal regime where analytical expressions are no longer valid [13], and IMD evaluation also plays a crucial role to define the optimal electrical data power range according to the optical system parameters.

In this article, for the first time to our knowledge, we present both theoretical and experimental comprehensive analysis of the mmW gain in photonically generated CS-MZM approach using a DML for signal transmission. An exhaustive analysis of the system response is provided under small and large signal regime where the system nonlinearities leading to intermodulation effects are fully identified at the transition point between both signal operation regimes. Accordingly, the obtained results are validated by testing the system performance over different signal conditions in order to exploit the benefits of this mmW gain for future deployment of higher energy efficient networks.

II. System Description for Large Signal Regime

In this section, an exhaustive investigation of the photonic mmW signal generation scheme based on external carrier suppressed modulation is presented under large signal regime. In our system, a DML is employed for transmitting data over the photonically generated mmW signal under remote configuration in a centralized network architecture, as was considered in our previous work [10], where analytical formulation of the system response was limited to small signal regime.

As depicted in Fig. 1, a DML located at the BBU in the CO emits an optical carrier centered at the angular frequency $\omega_0 = 2\pi f_0$ modulated by the signal data. In this case, a data generator (DG) provides a digital data sequence over the intermediate frequency f_{IF} as modulating signal in the DML with an electrical power P_{IF}. The resulting modulated optical signal is then launched into a polarization controller (PC) to adjust its polarization.

To evaluate the system response, we consider the laser direct modulation by a single tone at angular modulation frequency of $\omega_{IF} = 2\pi f_{IF}$. In this case, the output electric field of the DML can be described by [14]:

$$E_{DML}(t) = \sqrt{P_o\,(1 + m_{AM} \cdot \cos\omega_{IF}t)}\; e^{jm_{PM}\,\cdot\,\cos(\omega_{IF}t+\Delta\varphi)} e^{j\omega_0 t} \tag{1}$$

where P_o is the laser output power and m_{AM} and m_{PM} are the amplitude and phase modulation indexes, respectively. Note the parameter m_{AM} is directly proportional to the square root of P_{IF} which measurement provides a value of 0.1 for $P_{IF} = 0$ dBm in our experimental setup. The phase difference between amplitude and phase modulation introduced by the laser is $\Delta\varphi$. From [14], we obtain the equations for m_{PM} and $\Delta\varphi$ which are related to the linewidth enhancement factor, α, and adiabatic laser chirp, κ, as:

$$m_{PM} = \alpha m_{AM}\sqrt{1 + \left(\frac{\omega_C}{\omega_{IF}}\right)^2}\;\Delta\varphi = -\text{atan}\left(\frac{\omega_C}{\omega_{IF}}\right) \tag{2}$$

where $\omega_c = \kappa P_o$ is the DML characteristic frequency. This analysis requires numerical simulations to evaluate the system operation under large signal regime since the residual phase modulation produced in the DML is not negligible at low frequencies, concretely when $\omega_{IF} << \omega_c$, as shown in (2). Under this assumption, $\Delta\varphi$ tends to $-\pi/2$, i.e., frequency independent and therefore, the DML chirp is mainly affected by m_{PM}.

Then, a MZM driven by a $\omega_{RF} = 2\pi f_{RF}$ signal tone generated by a local oscillator (LO) and biased (V_{bias}) at the null point for carrier suppression is used to provide the signal up-conversion into the mmW band ($2f_{RF}$) after photodetection. The time response of the MZM is given by:

$$h_{MZM}(t) = \cos\left(\varphi_{DC} + 2m_{RF}\cos\omega_{RF}t\right) \tag{3}$$

where φ_{DC} is the phase signal change caused by DC bias ($\varphi_{DC} = \pi/2$ in carrier suppression) and m_{RF} is the RF modulation index.

The output signal is then launched into an erbium doped amplifier (EDFA) to compensate the optical losses and into an optical band pass filter (OBPF) to reduce the amplified

spontaneous emission (ASE) noise. The resulting signal is then transmitted over the standard single mode fiber (SSMF) link at the optical distribution network (ODN) and sent to an RRH through a variable optical attenuator (VOA) to control the received optical power (RoP) at the photodetector (PD) input port. According to the schematic depicted in Fig. 1, the input electric field at the photodiode, $E(t)$, is given by the convolution between the response of the dispersive element and the electric field after modulation, as follows:

$$E\left(t\right) = \left[E_{DML}\left(t\right) \cdot h_{MZM}\left(t\right)\right] \otimes h_{SSMF}\left(t\right) \tag{4}$$

where $h_{SSMF}(t)$ is the impulse response of the signal propagation in SSMF which can be expressed as [15]:

$$h_{SSMF}\left(t\right) = \frac{1}{\sqrt{j2\pi\beta_2 L}} e^{j\frac{\pi}{2\beta_2 L}t^2} \tag{5}$$

where L is the fiber length, and the dispersion parameter β_2 is the second derivative of the propagation constant with respect to the optical frequency at ω_0.

Finally, the optoelectronic conversion is carried out at the PD and then, followed by the vector signal analyzer (VSA) where system performance is evaluated. The electrical current $i(t)$ can be calculated from $E(t)$ at the input of the photodiode as:

$$i\left(t\right) = \Re \cdot P\left(t\right) = \Re \cdot \left|E\left(t\right)\right|^2 \tag{6}$$

where $\Re$ is the photodiode responsivity and $P(t)$ is the received optical power. The calculation of the photocurrent $i(t)$ in (6) leads to recover the mmW signal centered at $f_{mmW} = 2f_{RF} \pm f_{IF}$ for further analysis.

Using the theoretical analysis presented in [10] under small signal regime, the current amplitude response at low frequencies ($\omega_{IF} \cong 0$) can be obtained in the mmW band for OB2B and SSMF link under remote configuration from (17) and (19) in [10], respectively, as detailed in Table I:

TABLE I
CURRENT AMPLITUDE RESPONSE AT LOW FREQUENCIES IN THE MMW BAND (SMALL SIGNAL REGIME)

	$i(2\omega_{RF} \pm \omega_{IF})$	
OB2B	$\Re P_o m_{AM} m_{RF}^2 sin^2\varphi_{DC}$	(7)
SSMF	$\Re P_o m_{AM} m_{RF}^2 sin^2\varphi_{DC}(1 \pm j\alpha\kappa P_o \beta L\omega_{RF})$	(8)

Comparing both expressions of Table I, OB2B and SSMF scenarios lead to different electrical power level at low frequencies due to the chirp parameter of the DML and the dispersion over the RF subcarrier angular frequency ω_{RF}. We consider the system mmW gain defined as the ratio of such electrical power and P_{IF} as the input power:

$$G_{mmW} = \frac{\mathrm{Z}_o \left|\mathrm{i}\left(2\omega_{RF} \pm \omega_{IF}\right)\right|^2}{\mathrm{P}_{IF}} \tag{9}$$

where $\mathrm{Z_o}$ is the PD impedance. Then, the amplitude response for OB2B in (7) leads to $G_{mmW}(0)$, i.e., the fiber length $L = 0$, and $G_{mmW}(\mathrm{L})$, that can be obtained from (8), corresponds to the mmW gain over an L long fiber link under small signal regime. By substituting (7) and (8) in (9), the following relationship can be obtained between them:

$$G_{mmW}(L) = G_{mmW}(0)\left[1 + \left(\alpha\kappa P_o \beta L\omega_{RF}\right)^2\right] \tag{10}$$

From (10), we observe that the remote configuration leads to a relative mmW gain, $G_R = G_{mmW}(L)/G_{mmW}(0)$, that increases with the length of the fiber link. In principle, this property is interesting since it implies that the obtained SNR is higher in longer fiber links and consequently, the transmission performance also improves in terms of EVM due to the combination of the DML chirp and the fiber dispersion. However, this property may not be valid when large signal regime is considered, i.e., high electrical power of the modulating data at the DML (P_{IF}).

In order to evaluate the impact of the large signal regime over the scheme depicted in Fig. 1, the frequency system response was measured by using a single tone as modulating signal at the DML (see Fig. 2). With a fixed electrical power (P_{IF}), a frequency sweep of the signal tone (f_{IF}) is applied to the DML from $f_{IF} =$ 200 MHz up to 15 GHz. This experiment was carried out by using Rohde & Schwarz SMW200A as the DG and repeated with different P_{IF} values set for modulating the DML (Optical Zonu OZ516). The up-conversion of the signal was achieved by using the MZM Sumitomo T.DEH1.5-40X-ADCY-Z biased ($\mathrm{V_{bias}} = 7.5$ V) at the null point and driven by an $f_{RF} = 20$ GHz electrical single tone generated by signal generator (SG) Agilent 8267C. For the compensation of the optical losses and ASE noise filtering, the Amonics AEDFA-23-B-FA optical amplifier and the Alnair BVF-100 OBPF were used, respectively. After the SSMF link, a VOA (Thorlabs EVOA1550A) was used to control the RoP at the input of Finisar XPDV3120R PD regardless of the fiber length, i.e., link losses.

Finally, Rohde & Schwarz FSW43 VSA was used to analyze the recovered mmW signal at the frequency of interest $f_{mmW} = 2f_{RF} \pm f_{IF}$, which is limited to 43 GHz. For most real applications, note that just a single mmW carrier is needed to transmit, so a commercial high-pass band filter can be included at the RRH to transmit only the upper carrier at $2f_{RF} + f_{IF}$. However, the lower one is used along the manuscript to show the system performance without loss of generality since the system response is similar for both mmW bands.

Fig. 2(a) shows the OB2B electrical system response of the current amplitude after photodetection at the mmW band ($f_{mmW} = 2f_{RF} - f_{IF}$) for different P_{IF} levels, i.e., $P_{IF} = -10$, 0 and 10 dBm while RoP = 0 dBm was kept constant at the PD input. We observe that experimental results of the amplitude response at mmW band is equivalent to the DML frequency response [10] in good agreement with the simulation plotted by means of solid lines in Fig. 2(a). Non-significant differences are found in the frequency response apart from the subsequent signal increase over the whole frequency range according to the electrical signal power of the modulating signal (0, 10 and 20 dB with respect to the lower one). A 3 dB bandwidth close to 7.8 GHz is obtained in all cases, which is limited by the relaxation oscillation frequency of the laser, as its intrinsic characteristic. In Fig. 2(b), a 10 km SSMF link is considered with the

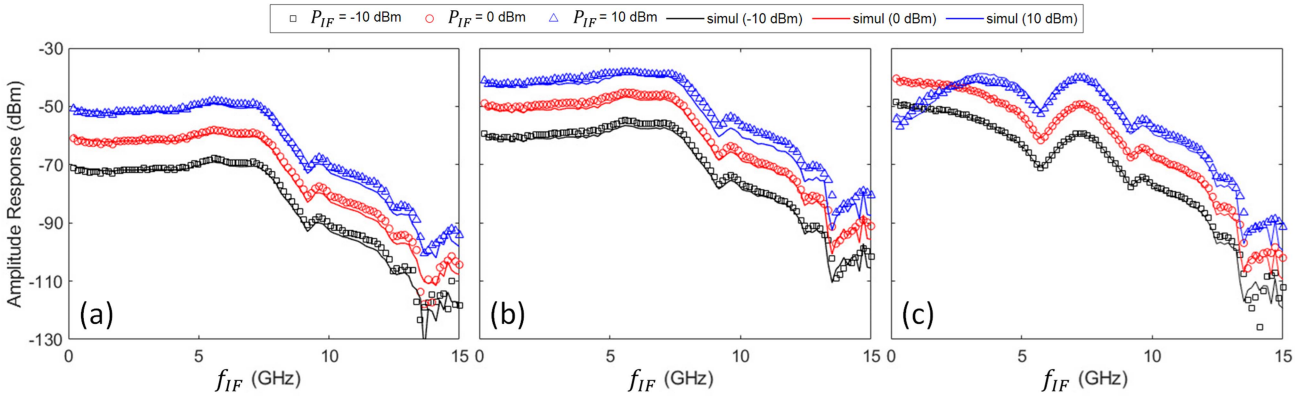

Fig. 2. Experimental electrical frequency response at the mmW band ($f_{mmW} = 2f_{RF} - f_{IF}$) for P_{IF} levels set at -10 (■), 0 (●) and 10 (▲) dBm: (a) OB2B, (b) 10 km SSMF link and (c) 35 km SSMF. Solid line refers to the corresponding simulation.

same RoP = 0 dBm. In this case, the frequency response depicts a slight variation of the 3 dB bandwidth, i.e., from 7.9 GHz to 8.1 GHz when the electrical power P_{IF} increases from -10 to 10 dBm, respectively. Besides, the combination of DML chirp and the fiber dispersion leads to a 12 dB relative mmW gain in the system response, i.e., with regard to OB2B configuration, for $P_{IF} = -10$ dBm whereas such gain decreases up to 10 dB when $P_{IF} = 10$ dBm. Note that optical losses of the fiber link are compensated to keep the RoP constant in order to provide a fair comparison of the system performance.

In order to provide further analysis, Fig. 2(c) shows the amplitude response when the fiber length is $L = 35$ km. Firstly, we observe relative mmW gain values (at low f_{IF}) around 22.7 and 20.5 dB for $P_{IF} = -10$ and 0 dBm, respectively. This gain is according to (10), so we can consider that the system operates under small signal regime. Although low-pass frequency is still present, the 3 dB bandwidth of the system response decreases down to 2.4 GHz in comparison to both OB2B and 10 km fiber link due to higher accumulated fiber dispersion in 35 km link. By contrast, a high-pass frequency response is observed for $P_{IF} = 10$ dBm, i.e., large signal regime, with a relative mmW gain reduced to values close to OB2B, i.e., $G_R = 1$ (0 dB) at low f_{IF}. Therefore, the frequency response shows an amplitude reduction of 26 dB at low frequencies in the mmW band between small and large signal regime. Note this high-pass effect is observed for frequencies up to 4.5 GHz due to a strong variation of the phase modulation produced in the DML at low frequencies according to (2) whereas the system response shows similar curves for IF frequencies higher than 4.5 GHz in spite of the power level regime.

By using general formulation (1)–(6), the numerically evaluated response is obtained with the parameters adjusted to those employed in the experimental setup, as detailed in Table II and a good agreement is obtained with measurements, as shown in Fig. 2.

For the sake of validation, Fig. 3 represents the relative mmW gain ($f_{IF} = 200$ MHz) for different P_{IF} levels and fiber lengths by keeping constant RoP = 0 dBm. It can be observed that the measured relative mmW gain (in linear units) exhibits a linear behavior versus L^2 under small signal regime, i.e., for $P_{IF} = -10$ dBm. In this case, both experimental measurements (plotted with symbols) and the simulated curve (solid line in black) have a linear behavior according to the theoretical prediction derived from (10), so we demonstrate that small signal regime model accurately describes the system gain obtained at mmW band. However, the gain decreases significantly with the increase of electrical power P_{IF} due to the cumulative fiber dispersion, making this model no longer valid. Indeed, Fig. 3 shows numerical results under large signal regime in good agreement with

TABLE II
PARAMETERS FOR THEORETICAL ANALYSIS

	Parameter	Value
DML	λ_0	1552.51 nm
	P_o	4 mW
	α	3.75
	κ	7.8 GHz/mW
MZM	m_{RF}	0.32
	φ_{DC}	$\pi/2$
	f_{RF}	20 GHz
SSMF	β_2	-22.1 ps^2/km

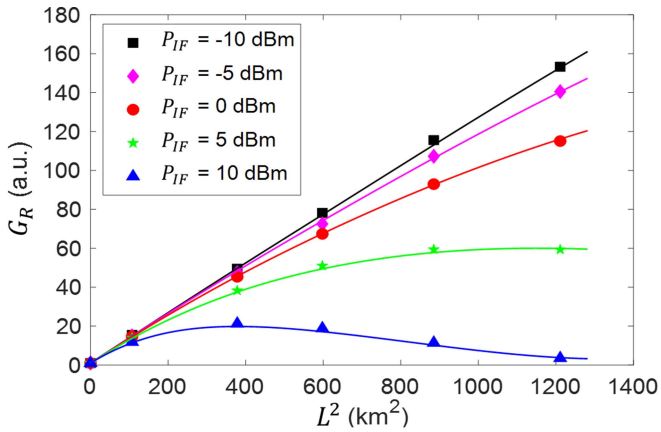

Fig. 3. Measurement of G_R at mmW band for different P_{IF} levels vs the square of the length of the fiber link. Experimental results are represented by symbols whereas solid curves are theoretical simulations.

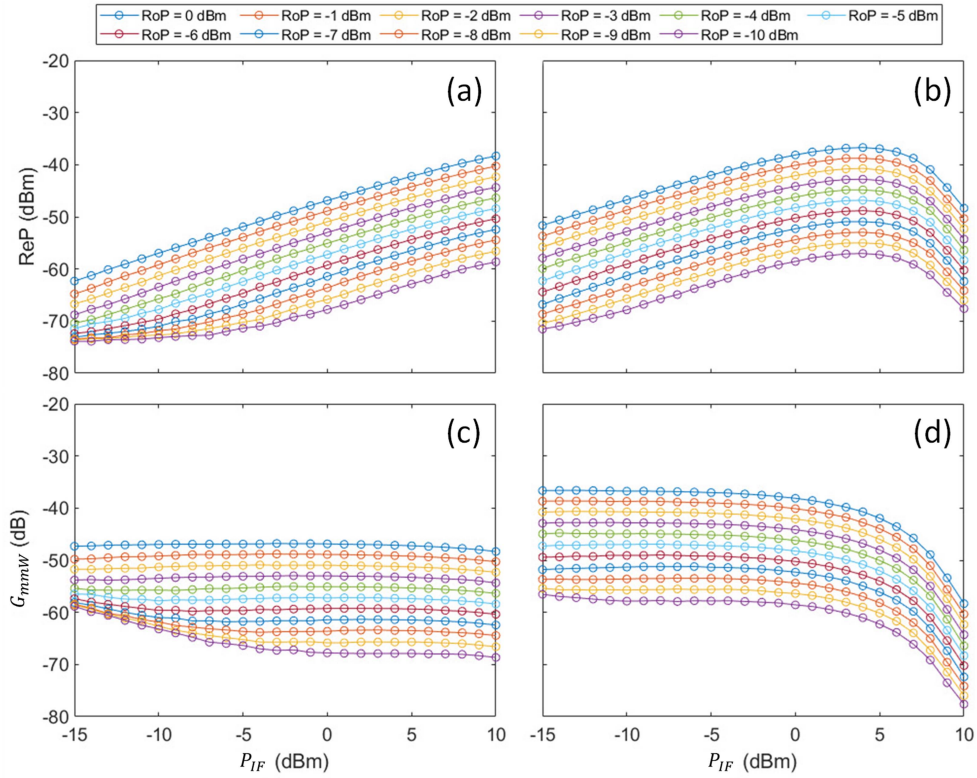

Fig. 4. (a)–(b) Experimental ReP vs P_{IF} at the DML and (c)–(d) mmW gain vs P_{IF} for 10 km (left) and 35 km (right) fiber lengths, respectively.

the experimental measurements far from the linear behavior. Moreover, we can observe that P_{IF} levels higher than 5 dBm lead to a maximum gain for a certain fiber length and even a drop-off of the mmW gain with respect to shorter fiber links.

III. Experimental Evaluation of System Performance

In this section, we analyze the system performance when data signal is photonically generated at $f_{mmW} = 2f_{RF} \pm f_{IF}$ under large signal regime. The local oscillator is given by $f_{RF} =$ 20 GHz, so the mmW band is located around 40 GHz.

In this experiment, a QPSK signal with a sample rate of 25 Mbps and a root-raised-cosine filter with a roll-off factor of 0.22 was generated at an intermediate f_{IF} of 200 MHz by using a vector signal generator (SMW200A) which permits to control the electrical data power, P_{IF}, applied to the DML. We compare the signal transmission of data carried by mmW frequency over 10 and 35 km fiber lengths when the electrical power P_{IF} is set from -15 to 10 dBm in order to identify the transition between small and large signal regimes.

Fig. 4(a) and (b) depict the received electrical power (ReP) at the VSA for different P_{IF} values over 10 and 35 km SSMF links, respectively. Different curves have been obtained by setting several RoP values in -10 to 0 dBm range. We notice that ReP increases linearly with P_{IF} in both cases according to (10) under small signal regime. A slight deviation is found for low P_{IF} values when RoP is lower than -6 dBm after 10 km fiber length due to the floor noise of the VSA which is -148 dBm/Hz, i.e., -74 dBm over 25 MHz measurement bandwidth. However, in

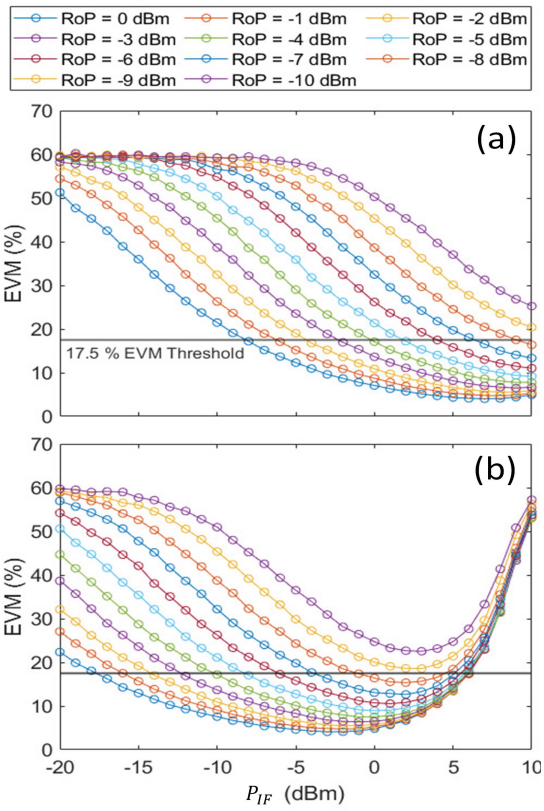

Fig. 5. Measured EVM vs P_{IF} at different RoP levels for: (a) 10 km and (b) 35 km fiber lengths.

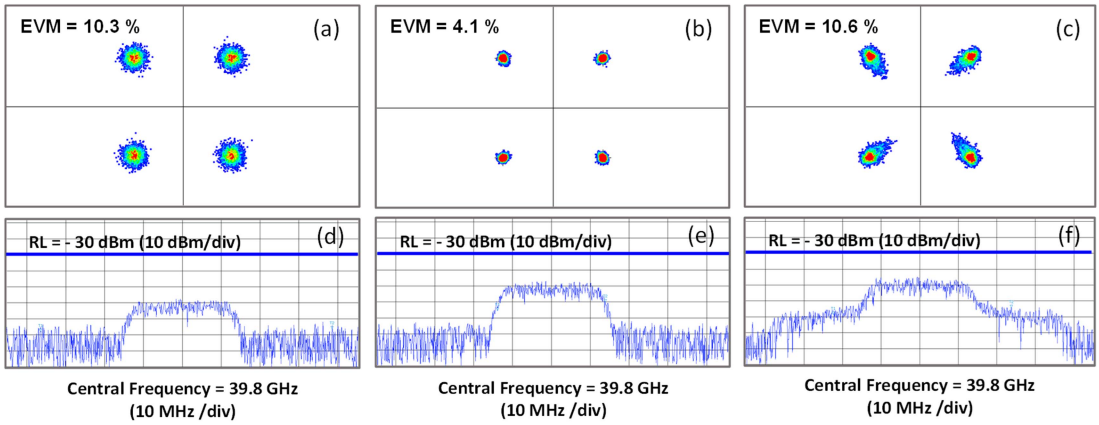

Fig. 6. Measured QPSK constellation for a 35 km long link (RoP = 0 dBm): (a) 10.3% EVM for $P_{IF} = -13$ dBm, (b) minimum EVM value (4.1%) achieved with $P_{IF} = -3$ dBm, and (c) 10.6% EVM for $P_{IF} = 4$ dBm. The corresponding electrical spectra are plotted in (d), (e) and (f).

the case of 35 km, the ReP decreases for P_{IF} values higher than 4 dBm, as observed for any RoP level. This behavior is corroborated when studying the mmW gain dependence on the electrical power P_{IF} and different RoP levels (see Fig. 4(c) and (d) for 10 and 35 km fiber lengths, respectively). Although both cases exhibit a constant gain, that is proportional to RoP, for low P_{IF}, it can be observed that 35 km leads to 10 dB higher gain than measured over 10 km, as expected from (10). Nevertheless, the gain of this link decreases for P_{IF} higher than 0 dB, down to 23 dB with respect to the constant level for $P_{IF} = 10$ dBm, which shows the system is operating under large signal regime.

Fig. 5(a) and (b) show the obtained error-vector-magnitude (EVM) after demodulating the transmitted data in the 40 GHz-band over 10 and 35 km fiber links, respectively, when different electrical power P_{IF} is employed. Note that 17.5% EVM threshold is plotted for QPSK signals according to [16]. Different curves represent the measurements taken under different RoP values in the -10 to 0 dBm range. Initially, the EVM performance for low operating P_{IF} is determined by the white noise performance of the RF system. Moreover, as it is well known, the EVM is inversely proportional to the signal-to-noise ratio SNR in decibel (dB) [17]. This behavior can be observed in all curves displayed in Fig. 5(a) for P_{IF} values lower than 10 dBm whereas in Fig. 5(b) this proportionality only occurs for P_{IF} values lower than 0 dBm. However, nonlinearities increase with the signal power, and consequently, the quality of the recovered signal decreases. Indeed, the system nonlinearities show significant impact on the EVM for high operating power level due to some intermodulation products which fall within the signal frequency band. Moreover, they can overlap with the electrical subcarriers with strong impact on their amplitude and phase [18], [19].

The total EVM level for a system is given by the addition of all these error sources also including the phase noise, as shown in Fig. 5(b). For instance, the lowest EVM level is 4.1% for a P_{IF} close to 7 dBm and -3 dBm for 10 and 35 km, respectively, when an RoP equal to 0 dBm is considered.

As an example, Fig. 6 exhibits the measured constellations and electrical power spectra for a 35 km SSMF link with RoP = 0 dBm where white noise, phase noise and intermodulation

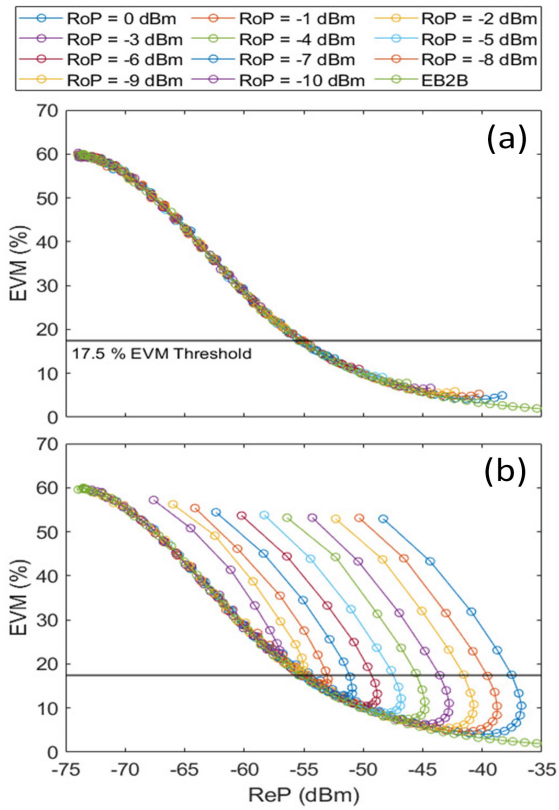

Fig. 7. Measured EVM values vs ReP levels for (a) 10 km and (b) 35 km SSMF links.

are present. Constellations around 10% EVM value are chosen to illustrate the impact of the white noise on the system performance for $P_{IF} = -13$ dBm, i.e., low operating power level (Fig. 6(a)), and the impact of the system nonlinearities when $P_{IF} = 4$ dBm, as prominent in high operating power levels (Fig. 6(c)). As a matter of fact, Fig. 6(a) shows an EVM value of 10.3% achieved with low P_{IF}, as opposed to 10.6% EVM value obtained for high P_{IF}, as depicted in Fig. 6(c). On the contrary, the transmission is optimized when the system

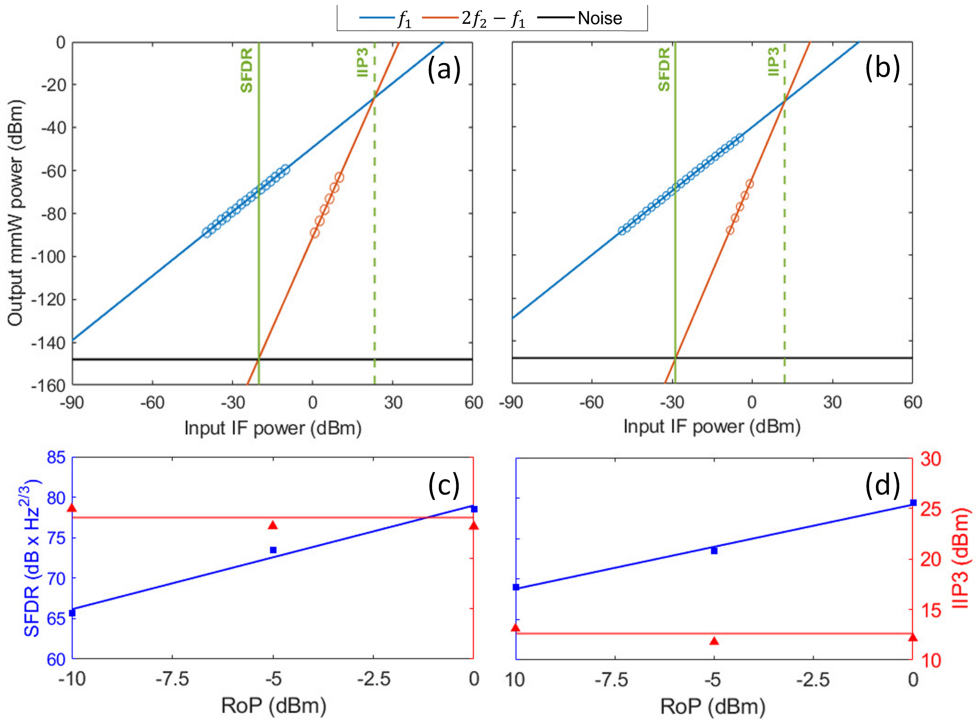

Fig. 8. Output power and SFDR calculation at mmW band vs P_{IF} when RoP is 0 dBm for (a) 10 km and (b) 35 km. Lower graphs correspond to SFDR ratios (■) and IIP3 (▲) levels vs different RoP values for (c) 10 km and (d) 35 km.

reaches an optimal input power level P_{IF} of -3 dBm which leads to a minimum EVM level of 4.1% (Fig. 6(b)). The effects of both white noise and system nonlinearities are also analyzed by means of the corresponding received electrical spectra. In Fig. 6(d) and (e), there is no evidence of any nonlinearity at a glance so white noise is the most prominent error source which is progressively minimized when the operating power level is increased up to -3 dBm. Note that the measured ReP in Fig. 6(d) and (e) is -49.6 and -40.3 dBm. For higher input P_{IF} level, the intermodulation products falling within the signal bandwidth are taking its toll on the recovered signal quality as shown in Fig. 6(f) compared to Fig. 6(d) with similar EVM level. In Fig. 6(f), the measured ReP is around -36.7 dBm.

In order to validate these measurements, Fig. 7 shows the EVM values obtained for each ReP level by changing P_{IF} for a fixed RoP, as presented in Fig. 5. In Fig. 7(a), we observe that the quality of the recovered signal is independent of the RoP level when considering a 10 km long fiber link. Each curve for fixed RoP shows values up to the maximum ReP value which is achievable for the maximum P_{IF} value. Indeed, the collected data overlaps the electrical back-to-back (EB2B) of the system, which demonstrates the transparency of our photonic up-conversion link (see Fig. 7(a)). Nonetheless, when observing the collected data in Fig. 7(b) for 35 km fiber length, we find a U-shaped curve because ReP levels are obtained by varying P_{IF} value. Note that higher power level P_{IF} leads to higher ReP values up to a certain maximum value as shown in Fig. 4(b). However, further increase of P_{IF} leads to lower ReP values because of increased nonlinearities that lead to intermodulation products falling around the signal bandwidth as depicted in Fig. 6(f). Note that EVM increases also slightly for ReP values from -35 to -45 dBm in Fig. 7(a). Indeed, Fig. 7(a) and (b) show similar behavior but such distortion appears from a minimum power level which is 10 dB higher for 10 km than 35 km fiber link. Therefore, we can only observe this multi-valued curve for 35 km within the P_{IF} available range in the experimental setup.

Finally, in order to compare the third-order intermodulation distortion (IMD3) between small and large signal regime, the measured spurious-free dynamic range (SFDR) ratio in 10 km and 35 km fiber links is presented in Fig. 8. Both signal and distortion bands located at the mmW frequencies $2f_{RF} - f_1$ and $2f_{RF} - (2f_2 - f_1)$, respectively, were measured by performing a power sweep of P_{IF} for a given RoP level. As Fig. 8(a) and (b) show, the SFDR ratio when RoP is 0 dBm has a similar value of 78.6 and 79.4 dB $\cdot$ Hz$^{2/3}$ for 10 and 35 km, respectively. Indeed, the SFDR ratio is proportional to the RoP level and shows similar tendencies for 10 and 35 km as depicted in Fig. 8(c) and (d), respectively. Moreover, the third-order intercept point (IIP3) was measured to identify small and large signal regime. Fig. 8(c) and (d) show also the IIP3 measurement with average values of 23.7 and 12.4 dBm for 10 and 35 km, respectively. This IIP3 difference, i.e., 11.3 dB is related to the differential gain between both scenarios with 10 and 35 km.

Fig. 9(a) and (b) represent the measured constellations for an RoP value of 0 dBm with the minimum EVM value when both 10 and 35 km SSMF links are considered, respectively. A minimum EVM value of 4.1% is obtained in both cases for an input P_{IF} value of 7 and -3 dBm for a 10 and 35 km fiber length, as expected from curves with RoP $= 0$ dBm in Fig. 5(a) and (b), respectively. These results are in very good agreement

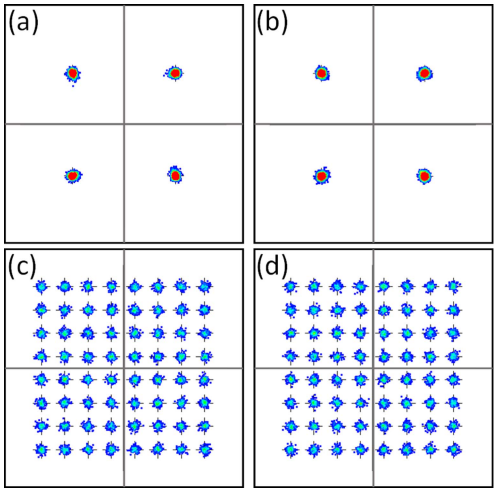

Fig. 9. Constellation diagrams measured at 10 km (right) and 35 km (left) for: (a), (b) QPSK and (c), (d) 64-QAM.

with the corresponding mmW gain depicted in Fig. 4(a) and (b), respectively. Similarly, Fig. 9(c) and (d) depict the constellation diagrams for 64-QAM for an RoP $=$ 0 dBm when 10 and 35 km transmission is performed for an input P_{IF} value of 7 and -3 dBm, respectively. All cases show an EVM value close to 4% with an ReP $= -40$ dBm since the design proposed in this manuscript permits to optimize properly the transmission quality for any modulation format.

IV. Conclusion

For the first time to the best of our knowledge, this article studies the mmW gain in a remote photonic signal generation approach both experimentally and theoretically by means of an exhaustive analysis based on CS external modulation of a DML under different signal regimes.

In order to validate the results, the mmW gain has been measured for different input electrical power levels, RoP values and fiber link lengths. Although the linear behavior of the collated data demonstrates that small signal regime model accurately describes the system gain, such gain decreases significantly with the increase of the P_{IF} level, thus making this model no longer valid under large signal regime. In all cases, a full agreement has been obtained between theoretical and experimental results. Therefore, the transition conditions to define different signal regimes depend on the accumulated dispersion and the input electrical power level. More specifically, the maximum gain values achieved for P_{IF} levels higher than 5 dBm is lower for longer fiber links, oppositely to systems operating under small signal regime.

In order to evaluate the system performance, the amplitude response at the mmW band has been measured for different scenarios in a centralized optical network. When OB2B is considered, i.e., no dispersive effects are present in the system, we have found that the electrical response is equivalent to the DML, i.e., the power of the mmW signal linearly depends on the input data electrical power level, as expected. However, when a fiber link is included under remote configuration, an improvement of the signal transmission is achieved due to the mmW gain arisen from the combination of the chirp characteristics of the DML and the chromatic dispersion of the fiber link. However, a considerable reduction of the mmW gain and the amplitude response bandwidth have been observed when the system is operating under large signal regime.

Furthermore, transmission experiments using a 25 MHz QPSK signal have been measured at mmW band around $2f_{RF} =$ 40 GHz to compare the system performance under small and large regime. As expected from theory, the quality of the transmitted signal is better for longer fiber links under small signal regime since the mmW gain is increased due to the interplay of the fiber dispersion and the DML chirp. The mmW gain leads to an improved SNR, and thus, a reduction of the measured EVM values.

The transmission results proved that white noise of the RF system determines the system performance for low operating P_{IF}. However, since the power of nonlinearities and intermodulation products rise when the signal power increases, a new phenomenon is observed for longer fiber links. Indeed, the recovered constellations and electrical spectra for 35 km SSMF clearly illustrate the effects of the white noise, phase noise and intermodulation when transition from small to large signal regime is held at 4 dBm electrical power. In our experimental setup, the system was always operating under small regime for 10 km SSMF because the transition is theoretically estimated around 14 dBm, which is far from the maximum experimental input electrical data power. Additionally, the transparency of our photonic up-conversion link is demonstrated by obtaining the performance characteristic, which overlaps with the EB2B under small signal regime.

Finally, the IMD3 between small and large signal regime has been compared by means of the SFDR and IIP3. Even though the SFDR results do not depend on the fiber dispersion, both small and large signal regime scenarios are determined by the IIP3 levels in each case. Once again, an IIP3 difference of 11.3 dB related to the different gain is observed between both scenarios with 10 and 35 km.

This article provides a key analysis for optimizing the design of highly energy efficient future communications networks. We have demonstrated that microwave photonic links with mmW signal generation provide a large signal gain over an electrical input power range which depends on the fiber dispersion and the laser chirp. Proper exploitation of this system gain allows to increase the energy efficiency of these networks, whereas the transition between small and large signal operation regime must be properly addressed to avoid intermodulation effects and gain reduction.

References

[1] ITU-R, "Report ITU-R M.2370-0; IMT traffic estimates for the years 2020 to 2030," 2015. [Online]. Available: https://www.itu.int/dms_pub/itu-r/opb/rep/R-REP-M.2370-2015-PDF-E.pdf

[2] Cisco, "Cisco annual internet report (2018–2023)," White paper, 2020. [Online]. Available: https://www.cisco.com/c/en/us/solutions/collateral/executive-perspectives/annual-internet-report/white-paper-c11-741490.html

[3] W. Jiang, B. Han, M. A. Habibi, and H. D. Schotten, "The road towards 6G: A comprehensive survey," *IEEE Open J. Commun. Soc.*, vol. 2, pp. 334–366, 2021, doi: 10.1109/OJCOMS.2021.3057679.
[4] C. Lim, Y. Tian, C. Ranaweera, T. A. Nirmalathas, E. Wong, and K.-L. Lee, "Evolution of radio-over-fiber technology," *J. Lightw. Technol.*, vol. 37, no. 6, pp. 1647–1656, Mar. 2019, doi: 10.1109/JLT.2018.2876722.
[5] I. A. Alimi, A. L. Teixeira, and P. P. Monteiro, "Toward an efficient C-RAN optical fronthaul for the future networks: A tutorial on technologies, requirements, challenges, and solutions," *IEEE Commun. Surveys Tuts.*, vol. 20, no. 1, pp. 708–769, Firstquarter 2018, doi: 10.1109/COMST.2017.2773462.
[6] C. Liu, J. Wang, L. Cheng, M. Zhu, and G.-K. Chang, "Key microwave-photonics technologies for next-generation cloud-based radio access networks," *J. Lightw. Technol.*, vol. 32, no. 20, pp. 3452–3460, Oct. 2014, doi: 10.1109/JLT.2014.2338854.
[7] J. Yao, "Microwave photonic systems," *J. Lightw. Technol.*, vol. 40, no. 20, pp. 6595–6607, Oct. 2022, doi: 10.1109/JLT.2022.3201776.
[8] C.-T. Lin, J. Chen, S.-P. Dai, P.-C. Peng, and S. Chi, "Impact of nonlinear transfer function and imperfect splitting ratio of MZM on optical up-conversion employing double sideband with carrier suppression modulation," *J. Lightw. Technol.*, vol. 26, no. 15, pp. 2449–2459, Aug. 2008, doi: 10.1109/JLT.2008.927160.
[9] H. Zhang, L. Cai, S. Xie, K. Zhang, X. Wu, and Z. Dong, "A novel radio-over-fiber system based on carrier suppressed frequency eightfold millimeter wave generation," *IEEE Photon. J.*, vol. 9, no. 5, Oct. 2017, Art. no. 7203506, doi: 10.1109/JPHOT.2017.2731620.
[10] L. Vallejo et al., "On the 40 GHz remote versus local photonic generation for DML-based C-RAN optical fronthaul," *J. Lightw. Technol.*, vol. 39, no. 21, pp. 6712–6723, Nov. 2021, doi: 10.1109/JLT.2021.3102818.
[11] L. Vallejo, J. Mora, and B. Ortega, "Harmonic and intermodulation distortion analysis in directly modulated lasers over local and remote photonically generated millimeter-wave signals," *J. Lightw. Technol.*, vol. 40, no. 15, pp. 5128–5140, Aug. 2022, doi: 10.1109/JLT.2022.3172771.
[12] N. Bamiedakis, D. G. Cunningham, and R. V. Penty, "Linearisation method of DML-based transmitters for optical communications part II: Experimental demonstration and implementation methods," *J. Lightw. Technol.*, vol. 39, no. 18, pp. 5828–5836, Sep. 2021, doi: 10.1109/JLT.2021.3093845.
[13] E. Peral and A. Yariv, "Large-signal theory of the effect of dispersive propagation on the intensity modulation response of semiconductor lasers," *J. Lightw. Technol.*, vol. 18, no. 1, pp. 84–89, Jan. 2000, doi: 10.1109/50.818911.
[14] L. A. Neto et al., "Simple estimation of fiber dispersion and laser chirp parameters using the downhill simplex fitting algorithm," *J. Lightw. Technol.*, vol. 31, no. 2, pp. 334–342, Jan. 2013, doi: 10.1109/JLT.2012.2226704.
[15] I. P. Kaminow, T. Li, and A. E. Willner, *Optical Fiber Telecommunications Volume VIB: Systems and Networks*, 6th ed. New York, NY, USA: Academic, 2013.
[16] ETSI, "5G; NR; user equipment (UE) radio transmission and reception; Part 2: Range 2 standalone," 3GPP, Sophia Antipolis, France, Tech. Specification 38.101-2 version 15.7.0 release 15, 2019.
[17] N. Argyris et al., "A 5G mmWave fiber-wireless IFoF analog mobile fronthaul link with up to 24-Gb/s multiband wireless capacity," *J. Lightw. Technol.*, vol. 37, no. 12, pp. 2883–2891, Jun. 2019, doi: 10.1109/JLT.2019.2897109.
[18] C. Lim, A. Nirmalathas, K.-L. Lee, D. Novak, and R. Waterhouse, "Intermodulation distortion improvement for fiber–radio applications incorporating OSSB+C modulation in an optical integrated-access environment," *J. Lightw. Technol.*, vol. 25, no. 6, pp. 1602–1612, Jun. 2007, doi: 10.1109/JLT.2007.896814.
[19] J. Wang, C. Liu, M. Zhu, A. Yi, and G.-K. Chang, "Closed-form analysis of intra/inter-band cross-modulation in multiband radio-over-fiber systems," in *Proc. IEEE Glob. Commun. Conf.*, 2013, pp. 2454–2460.

M. Botella-Campos received the B.Sc. degree in telecommunications systems, sound and image engineering and the M.Sc. degree in telecommunication technologies, systems and networks in 2019 and 2021, respectively, from Univertat Politècnica de València (UPV), Valencia, Spain, where she has been working toward the Ph.D. degree with Instituto de Telecomunicaciones y Aplicaciones Multimedia, Photonic Research Labs, Telecommunication Engineering Program since 2021. Her research interests include microwave photonics, mmW generation, RoF/FSO for 5G and beyond, and optical networks.

J. Mora received the M.Sc. degree in physical sciences and the Ph.D. degree in physics from the Universitat de València, València, Spain, in 1999 and 2005, respectively. From 1999 to 2004, he was with the Department on Applied Physics, Universitat de València. Since 2004, he has been a Senior Researcher with the Photonics Research Labs, Institute of Telecomunications and Multimedia (ITEAM), Universitat Politècnica de València. He has collaborated in many regional, national and international R&D projects involving research and industry. He is/was the Co-Founder of the UPV spin-off company EPHOOX in 2016, specialized on advanced instrumentation for Microwave Photonics and Radio over Fiber systems. With an H-factor of 25, he has authored or coauthored more than 100 papers and conference contributions in his research fields, which include using photonic technology (fibre bragg gratings for sensing applications, optical signal processing, microwave photonics, reconfigurable and convergent optical for wired/wireless services and quantum cryptography). He was the recipient of the Extraordinary Doctorate Prize of the Universitat de València in 2006.

B. Ortega (Senior Member, IEEE) received the M.Sc. degree in physics from the Universidad de Valencia, Valencia, Spain, in 1995, and the Ph.D. degree in telecommunications engineering from the Universidad Politécnica de Valencia, Valencia, in 1999. She is currently with the Departamento de Comunicaciones, Universitat Politècnica de València, where she holds a Full Professorship since 2009 and collaborates as a Group Leader with the Photonics Research Labs, Institute of Telecommunications and Multimedia Applications. She has authored or coauthored more than 200 papers and conference contributions in fibre Bragg gratings, microwave photonics and optical networks. She has got several patents and is also a co-founder of EPHOOX company. She has participated in a large number of European Networks of Excellence and R&D projects and other national ones. Her research interests mainly include optical devices, optical networks, and microwave photonic systems and applications.